SANDIA REPORT
SAND2014-17691
Unlimited Release
September 2014

Results from field tests of the one-dimensional Time-Encoded Imaging System

Jim Brennan,
Erik Brubaker,
Peter Marleau,
Aaron Nowack,
Patricia Schuster

Sandia National Laboratories

Prepared by Peter Marleau
Sandia National Laboratories
Albuquerque, New Mexico 87185 and Livermore, California 94550

Sandia National Laboratories is a multi-program laboratory managed and operated by Sandia Corporation, a wholly owned subsidiary of Lockheed Martin Corporation, for the U.S. Department of Energy's National Nuclear Security Administration under contract DE-AC04-94AL85000.

Issued by Sandia National Laboratories, operated for the United States Department of Energy by Sandia Corporation.

SAND2014-17691
Unlimited Release
September 2014

Results from field tests of the one-dimensional Time-Encoded Imaging System

Jim Brennan
Erik Brubaker
Peter Marleau
Aaron Nowack
Patricia Schuster

Radiation and Nuclear Detection Systems
Sandia National Laboratories
P.O. Box 969
Livermore, California 94551-MS9406

Abstract

A series of field experiments were undertaken to evaluate the performance of the one dimensional time encoded imaging system. The significant detection of a Cf252 fission radiation source was demonstrated at a stand-off of 100 meters. Extrapolations to different quantities of plutonium equivalent at different distances are made. Hardware modifications to the system for follow on work are suggested.

ACKNOWLEDGMENTS

This work was supported by NA-221, the office of non-proliferation R&D of the NNSA.

CONTENTS

FIGURES

TABLES

NOMENCLATURE

DOE	Department of Energy
HDPE	High Density Polyethylene
keVee	kilo-electronVolt electron equivalent
LS	Liquid Scintillator
MCNP	Monte Carlo N-Particle
MeVee	Mega-electronVolt electron equivalent
MLEM	Maximum Likelihood Expectation Maximization
PMT	Photomultiplier Tube
PSD	Pulse Shape Discrimination
RPM	Revolutions Per Minute
SNL	Sandia National Laboratories
SNM	Special Nuclear Material
WGPu	Weapons Grade Plutonium

1.0. INTRODUCTION

We have developed a neutron detector system based on time-encoded imaging and demonstrated its applicability to Special Nuclear Material (SNM) detection. Other imaging methods require either multiple interactions, leading to an intrinsically low efficiency, or spatial modulation of the signal, which requires a position sensitive detector and often leads to complicated and expensive designs. In contrast, a single detector using a time-modulated collimator can encode directional information in the time distribution of detected events. Time modulation as a means of directional discrimination, or imaging, has been an underexplored method for both gamma rays and especially high energy neutrons. This is the first investigation of time-encoded imaging for nuclear nonproliferation applications.

We foresee two transformative advantages of time-encoded imaging. One is that a new design space is opened for effective and low-cost directional detection. Time-encoding systems can have a low channel count, reducing cost and increasing robustness by simplifying system integration and calibration. They have intrinsically high efficiency, since only a single particle interaction is required and the detector size is scalable ranging from a handheld detector up to the large detector size (1000s of cm^2 effective area) needed for large standoff. The second advantage is that, with time encoding, the angular resolution of the image reconstruction depends primarily on the collimator design. It is effectively decoupled from the method used for particle detection, which drives the detection efficiency as well as the energy resolution for gamma events. Thus in a time-encoding imager both angular resolution and energy resolution can be independently optimized.

We have demonstrated the time-encoded imaging concept applied to standoff SNM detection with a prototype system and with simulated results. Here we report the results from field tests of a 1-D prototype system. In Section 2.0 we briefly describe the detection system and its calibration. Section 3.0 outlines the measurements that were made, Section 4.0 describes the analysis methods, and results are reported in Section 5.0.

2.0. TIME-ENCODED NEUTRON IMAGING SYSTEM

In order to take full advantage of the TEI approach for SNM detection via fast neutron signatures, we have investigated the use of large liquid scintillator (LS) cells as TEI detection elements. Various cell configurations were studied, primarily using different photomultiplier tube (PMT) candidates. Scintillation light collection from the cell and PMT characteristics were identified as the most important variables. Comparisons between different cell configurations, and a description of the selected cell configuration, a 11”D x 15” LS volume coupled to three 5” PMTs, are described in further detail in ref (1) and illustrated in Figure 1.

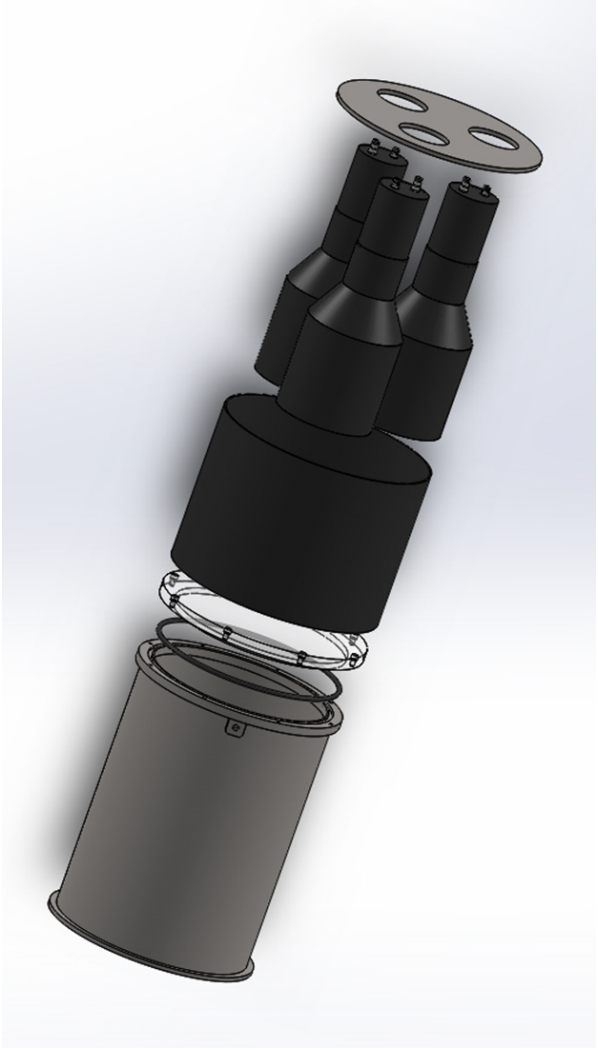

Figure 1 – Illustration of one of the large volume LS cells. Three 5" photomultiplier tubes are coupled to an 11" diameter X 15" deep cylinder of liquid scintillator. Signals in the three PMTs are summed for energy and PSD.

The Time-Encoded Neutron Imaging System (seen in Figure 2) consists of four such LS cells arranged in a diamond pattern optimized to enhance signal over background for the detection of weak point sources (2). The cells share an expansion reservoir to remove the need for a bubble within the sensitive volume. The cells, reservoir, and a VME crate containing a 16 channel digitizer (Struck SIS3316), and an HV power supply (ISEG) are all affixed to a turn table that is rotated by an electric motor controlled by the data acquisition computer. The rotation position is independently measured by an encoder. Signals from the PMTs are digitized by the Struck digitizer (3). As the detectors are rotated about a common axis, their signals become modulated as each cell occults the others along the line of site to a radiation source.

Figure 2 – Photograph of the Time-Encoded Imaging System. The four LS cells (center) and VME electronics crate (top) rotate together on the turn table (bottom). The entire system is controlled by a single laptop (right).

2.1. Calibrations

The combined signal from three PMTs has enhanced photo-collection efficiency and the relatively high quality (timing and gain) of the H6527 PMTs provides improved photo-statistics over previous designs. This provides good pulse shape discrimination (PSD) even in this large cell volume. In ref (1) we demonstrate >90% neutron efficiency with 99.99% gamma rejection above a 250 keVee threshold. In addition, it has been shown that there is no azimuthal asymmetry in the response of the detector and only ~20% gain variation along the height of the cell (though this is irrelevant to the performance of the detection system).

All three PMTs in each LS cell are gain matched. The Compton pulse height spectrum from a ^{22}Na gamma-ray source is used to match the gains of every PMT. Further, the spectrum is fit using a Monte Carlo spectrum and energy smearing terms as seen in Figure 3. This provides a measure of the gain and energy resolution that can be used in Monte Carlo simulations of the detector response.

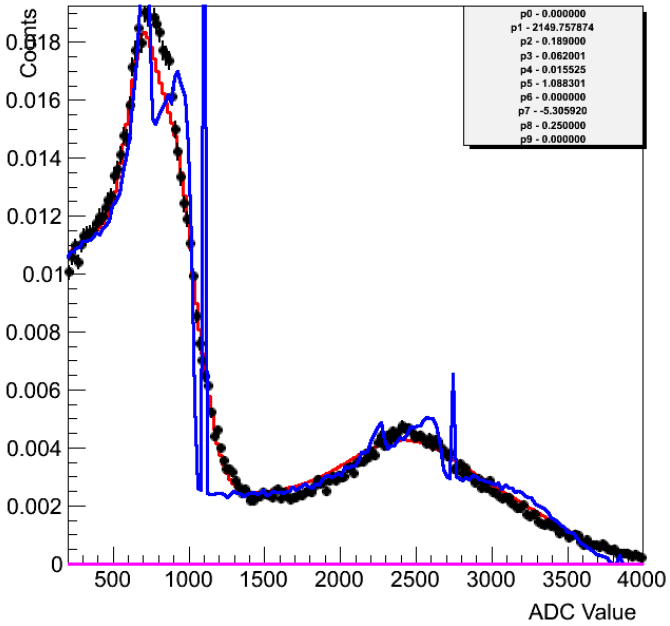

Figure 3 – The measured pulse height spectrum from a single PMT (black), the expect true energy deposition from a Monte Carlo simulation (blue), and the fit spectrum obtained by smearing the simulated spectrum (red).

Next, calibrations measurements were obtained using a ^{252}Cf fission source in order to establish discrimination cuts based on pulse shape. Figure 5 is an example of the one such calibration. A pulse shape discrimination (PSD) parameter is determined as the ratio of a tail integration to a total integration of the sum of the three PMT pulses. This is then plotted against the pulse height and a pulse height dependent cut is determined based on the requirement that an event have 4 sigma significance (99.99% probability) of being a neutron and not a gamma-ray.

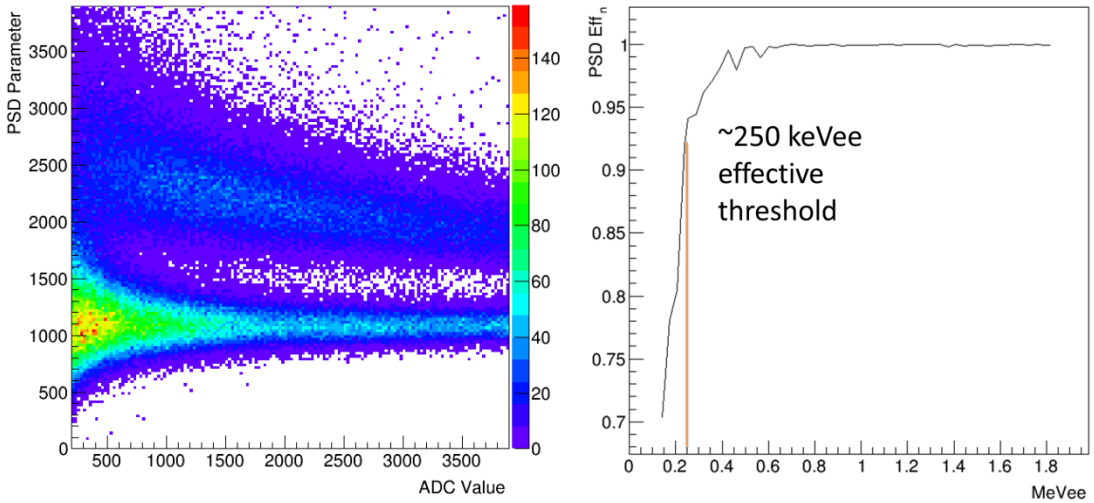

Figure 4 – (Left) PSD distribution for one of the LS cells. (Right) Relative efficiency of the 99.99% neutron probability cut as a function of energy (MeVee) indicating a 250 keVee threshold was achieved.

The results shown in Figure 4 were obtained soon after the completion of the LS cells. Unfortunately it was found late in the field testing that the liquid scintillator had been poisoned. This occurs when air makes its way into the cells and oxygen diffuses into the liquid scintillator. The degradation of PSD is evident by comparing PSD calibration data taken after field testing shown in Figure 5 to that found in Figure 4 (left).

We have identified that this problem was likely caused by the extreme temperature fluctuations encountered during the field tests. The TEI system spent several months from November 2013 to April 2014 in a trailer in a field at SNL Livermore during which the temperature ranged from near freezing to over 90F. Some amount of temperature fluctuation was anticipated and an expansion chamber (seen in Figure 6) was designed to allow for the liquid scintillator to expand and contract. However, when it became particularly cold, the chamber reached its minimum volume and began drawing air into the system.

This was identified as a problem when time modulation of the neutron rates was detected in background measurements as the bubble that formed in the cells oscillated with the rotation of the system. The bubbles were removed, but the poisoning had already occurred. Because of this, the effective energy threshold changed from 250 keVee to ~500 keVee and therefore we saw approximately half the sensitivity over the fission energy neutron spectrum than expected.

In follow on designs, this problem has been overcome with an expansion chamber designed for a larger volume range as well as keeping an overpressure of inert gas on the chamber such that, if bubbles do form in the cells, they will not poison the scintillator.

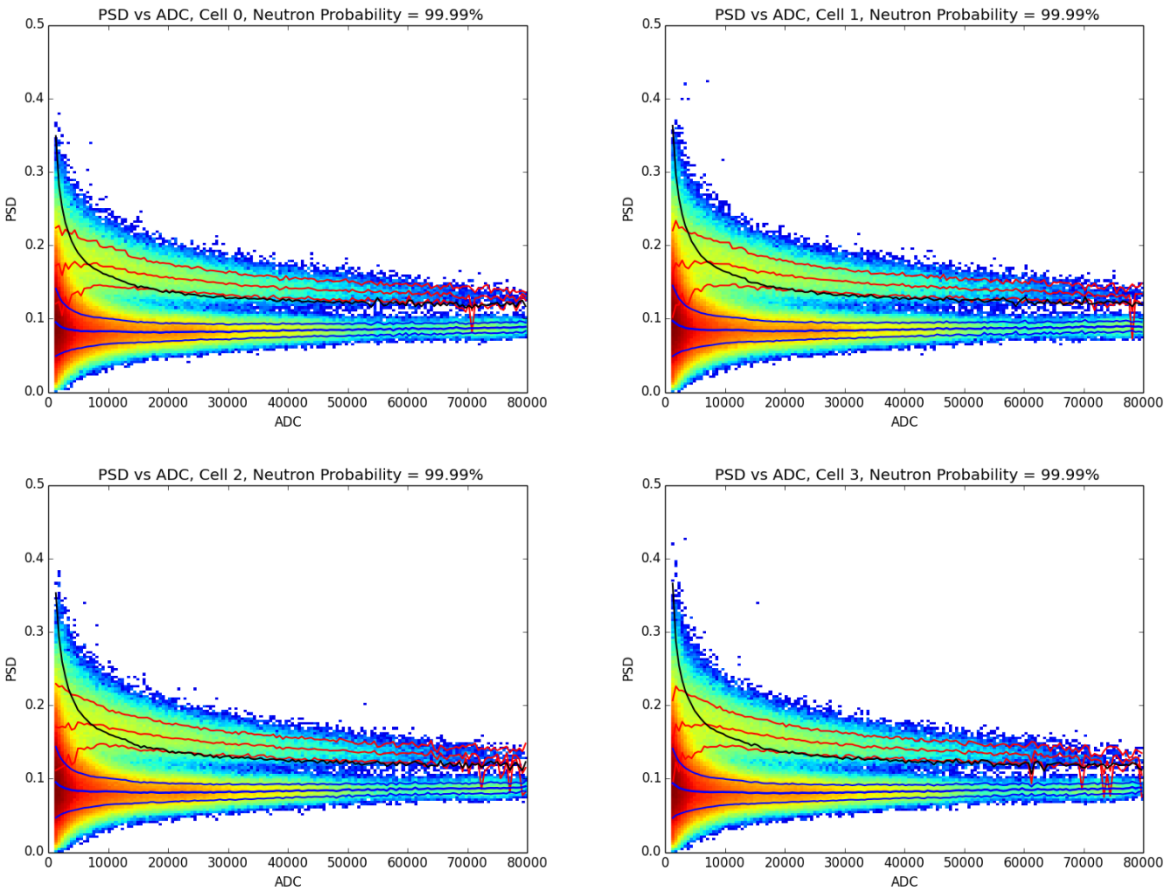

Figure 5 – The measured pulse shape parameter vs. pulse height for the four LS cells. Neutron/proton recoils lie within the upper band defined by the red lines (middle red line is the mean and top and bottom red lines contain 3 sigma deviations from the mean) while gamma/electron recoils fall in the lower band defined by the blue lines (middle blue line is the mean and top and bottom blue lines contain 3 sigma deviations from the mean). The black line between the two distributions represents the division between >99.99% probability of being neutron.

Figure 6 – Photograph of the liquid scintillator expansion chamber. Each of the four cells share this chamber to account for temperature dependent volume changes.

3.0. MEASUREMENTS

As can be seen in Figure 7 and Figure 8, the 1-D TEI system was installed into a 20 foot long trailer and parked in a remote corner of Sandia National Laboratories, CA for a series of large stand-off experiments. A container and stand (approximately 4ft in height as seen in Figure 9) were constructed to securely house one or several Cf252 fission sources. In Figure 8, the source container and stand can be seen in the distant background, 100 meters from the trailer and detection system. There was very little obstruction along the line of sight to the source.

During measurements the detector system continuously buffers data within the SIS3316 digitizers over one full rotation. After each rotation (operated at ~1 RPM), the detector is halted and the entire buffer is written to hard disk. This allows for close synchronization of positional information recorded by the encoder to the data recorded for each revolution without having to use multithreaded acquisition software. However, because of this decision, the system maintained an average dead-time of ~25%. In future iterations of this system, multithreaded data acquisition software will eliminate this dead-time.

Figure 7 – Photograph of the TEI system installed in a 20 ft. trailer for field measurements.

Figure 8 – Photograph of the 20 ft. trailer containing the TEI system. The Cf252 neutron source is contained in the locked shipping container that can be seen 100 meters behind the trailer in the empty field.

Figure 9 – Photograph of the locked container in which the Cf252 neutron source is installed for field demonstrations.

For all measurements described in the remainder of this report, one or multiple 35 microCurie Cf252 fission sources were used. For the preliminary 10 meter stand-off tests, a single source provided more than adequate signal to background. For the 100 meter stand-off tests, two such sources were paired together to enhance the signal. Even so, 70 microCuries of Cf252 emits ~2.8e5 n/s which is approximately 60% of the output of a significant quantity of WGPu as defined by the IAEA (8 kg). Therefore, the results presented in Section 5.0 could be achieved in 60% of the time for 8 kg of WGPu.

4.0. ANALYSIS

Before detection assessment and image reconstruction, all data is preprocessed. In the preprocessing step, pulses are converted into a measure of the energy deposited (in MeVee) using energy calibrations and a pulse shape parameter is extracted based on the ratio of the integral of a tail region of the pulse to the total charge integral. This parameter is then used to estimate the probability that each event is a neutron vs gamma-ray interaction based on the calibrations described in Section 2.1. Each event is time sorted and matched to a rotation angle based on the time stamp of the event and a time tagged list of encoder positions.

The result of the preprocessing step is four arrays (or histograms) of neutron counts vs. rotation angle, one for each LS detector. This is corrected for the time spent at each rotation angle and converted into neutron rates vs. rotation angle. Due to uneven amounts of time spent accelerating and decelerating as well as slippage in the drive wheels, the dwell time as a function of rotation angle frequently is not flat.

Lastly, these neutron rates vs. rotation angle can either be compared directly to what one would expect if only background is present (i.e. flat) or unfolded to produce a 1-dimensional image. In

the first case, any modulation statistically inconsistent with a flat distribution may be an indication of one or more sources present. Further, if the assumption is made that only a single point source might be present, then the expected (calculated) modulation as a function of angle can be tested against in the neutron rates. This so called "hypothesis test" is used to calculate the significance that a point source is present as a function of assumed angular location of the source as opposed to the presence of only background.

In order to unfold a 1-dimensional image, we use the Maximum-Likelihood Expectation-Maximization (MLEM) (4) algorithm. In this method, a detector response matrix is used to forward project an assumed neutron source distribution over the 1-dimensional space to a predicted set of neutron measurements. The algorithm then provides an update to the source distribution based on a comparison between the measured and forward projected values. Each iteration of this updating procedure is statistically guaranteed to increase the likelihood that the source distribution produces the measured rates.

The detector response matrix is constructed using MCNP-PoliMi (5) simulations of neutrons transported through the HDPE mask as a function of angular position. A neutron ring source with 60 meter radius with momentum directed in a cone toward the detector system and fission energy spectrum is used. It is assumed that 60 meters is large enough compared to the size of the detector system that the resulting response can be used for any "far field" measurement.

5.0. RESULTS

5.1. Background

As a point of comparison to the neutron source runs, 7 days of background data was acquired. This large data set is then sub-sampled to achieve a desired dwell-time. Figure 10 and Figure 11 show a random 30 minute and 1 hour sampling of this background respectively. It can be seen that no modulation is detected in these measurements and they reconstruct to a relatively flat source distribution using the MLEM routines as one would expect from an isotropic angular distribution.

A neutron rate between 1.4 and 2.0 neutrons per second per LS detector were measured with variability of 20-30% over the course of weeks. This variability would be a significant problem for weak or distant source detection if one were to rely on count rates alone. In Figure 11 (left) it can be seen that when the measurements were taken with a source at 100 meters, the background was approximately 30% higher than when the original background measurement was taken. Therefore, a background measurement taken weeks earlier cannot be assumed to be a good representation of what might be found on any given day. This highlights a major feature of time encoded imaging; the background is measured and estimated concurrent with the source.

5.2. Ten meter stand-off

In order to estimate the TEI system's detection sensitivity, a single ^{252}Cf source (~1.4e5 n/s) was measured at a 10 meter stand-off. Figure 10 shows the measured neutron rates and MLEM unfolded image as compared to background. At this distance and signal to background ratio, the

neutron rate modulation is clearly evident and the correct source location is apparent in the MLEM reconstructed image.

Based on the source's neutron emission rate, distance to source, average cross sectional area of the detector system (~2440 cm^2), and the measured modulation rate above background, we estimate an average detection efficiency of ~38% per cell averaged over the fission energy spectrum. When averaged over the entire detector system, this predicts an effective area of ~880 cm^2 (equivalent area of a 100% efficient detector). Although this value is relatively large, it is almost half the efficiency that was predicted during the design phase. This is most likely due to the oxygen poisoning of the liquid scintillator and resulting higher energy threshold that was discussed in Section 2.1.

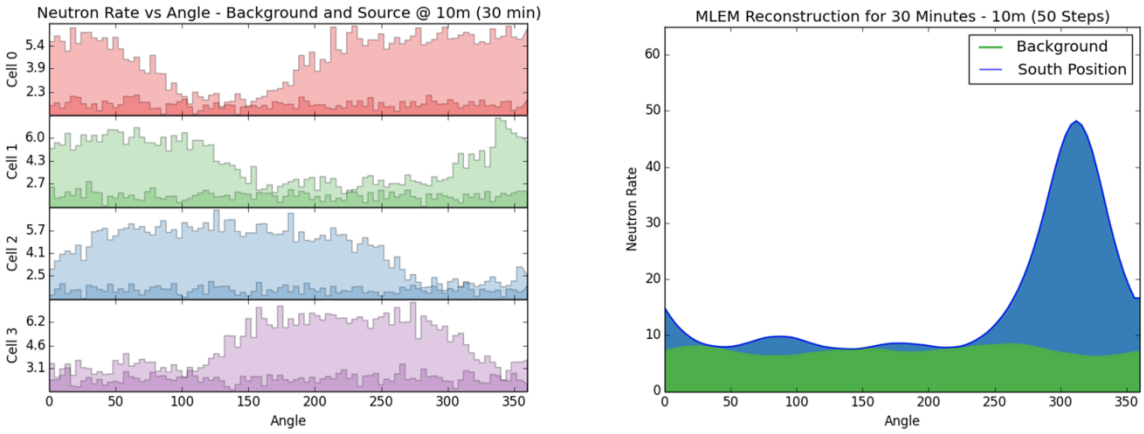

Figure 10 – (Right) Neutron rates in each of the four LS cells as a function of rotation angle for a Cf252 source at 10m. stand-off (light background colors) and background (darker foreground colors). (Left) MLEM reconstructed source distribution over azimuthal angles using these neutron rates for the Cf252 source (blue) and background (green). All measurements were taken with 30 minute dwell-time.

5.3. One hundred meter stand-off

To demonstrate the detection capabilities of the system over large stand-off distances, two collocated ^{252}Cf sources with combined strength ~2.8e5 n/s were measured at a 100 meter stand-off. The plots shown in Figure 11 reflect a random 1 hour of raw neutron rates vs. background rates (left) and the MLEM reconstructed source distributions (right). By eye, it is difficult (but not impossible) to detect modulation in the neutron detection rates. The MLEM analysis reveals an excess in the correct location, but by this image alone, it would also be difficult to claim detection. Therefore, we implemented the hypothesis test analysis that was discussed in Section 4.0. The results of this analysis shown in Figure 12 indicate significant detection of the source (>5 sigma) at the expected location in only a 30 minute measurement period.

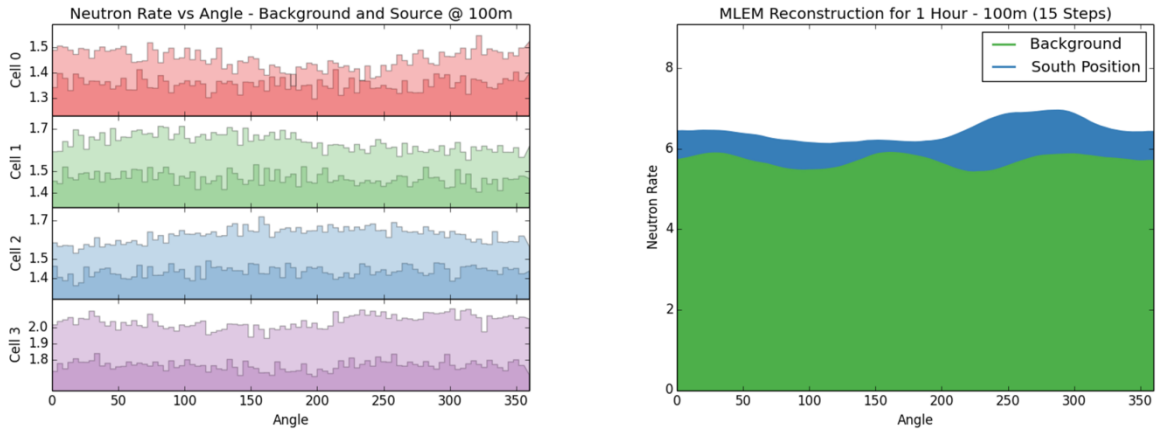

Figure 11 – (Right) Neutron rates in each of the four LS cells as a function of rotation angle for a Cf252 source at 100m. stand-off (light background colors) and background (darker foreground colors). (Left) MLEM reconstructed source distribution over azimuthal angles using these neutron rates for the Cf252 source (blue) and background (green). All measurements were taken with one hour dwell-time.

Given the estimated effective area, it was expected that the TEI system should have detected the source with ~5 sigma significance in approximately 15 mins. This discrepancy is likely attributed to systematic uncertainties in the response of the detector system. For instance, the MCNP simulations that were used to generate the system response matrix did not include features such as the cell window, PMTs, brackets, rotation table, frame, etc. Some of these features may contribute to the angular modulation of the system. Improvements in the detector response matrix are expected to improve the detection significance.

If scaled to an IAEA significant quantity of WGPu, the performance that was measured represents a 5 sigma significant detection over background in ~19 minutes. If the original PSD performance could have been maintained (approximately twice the sensitivity as discussed in Sections 2.1 and 5.2), it is estimated that this could have been achieved in ~9.5 minutes. Finally, if systematic uncertainties could be reduced through improvements in the system response matrix, this could potentially be reduced to as few as ~5 minutes.

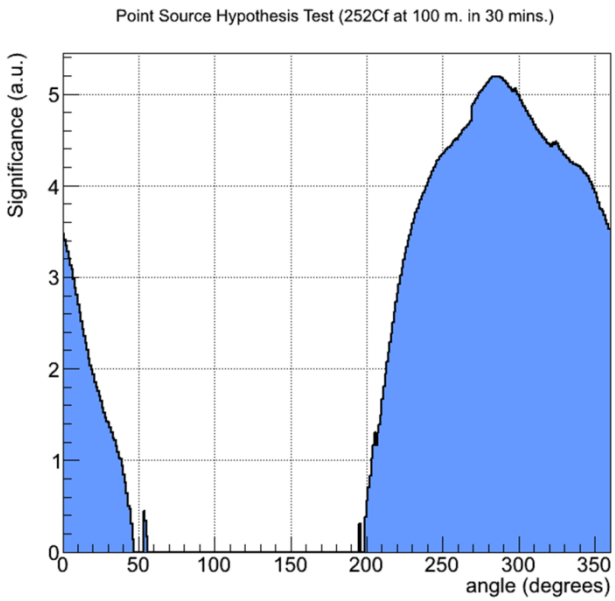

Figure 12 – Result of the point source hypothesis test as a function of the assumed angular position of the source.

6.0. CONCLUSIONS

Through a series of field tests with a prototype TEI system, we have successfully demonstrated significant detection (>5 sigma) of a 2.8e5 n/s neutron fission source at 100 meters stand-off in 30 min. In contrast to simple counting detectors, this was accomplished without the need of previous background measurements. Detection is accomplished without prior assumptions about expected count rates or background modeling. We expect that as we eliminate systematic uncertainties in the detector response matrix, the time to detection for this source strength could be reduced to as low as 15 minutes. If the LS detector performance established in preliminary laboratory tests could have been maintained throughout the field tests, the time to detection could potentially have been reduced by as much as a factor of two.

Over the course of these field tests, a series of technical challenges were encountered that had to be overcome. The next iteration of the TEI detection system is currently being developed for the purpose of area sweeping in a technical demonstration. These challenges are being addressed in this follow on project by implementing the solutions listed in Table 1. If successful, we anticipate performance on the level of significant detection of an IAEA significant quantity of WGPu at 100 meters in 5-7 minutes. For area sweeping applications, only stand-off distances on the scale of a building or high bay are required. In the same dwell time, as little as 300 grams of WGPu should be detectable within 20 meters of the system.

Table 1 – List of technical challenges and solutions being implemented.

Technical challenge encountered	Solution(s) being implemented
Liquid scintillator performance degraded as oxygen made its way into the system	1. Larger expansion volumes to handle larger temperature ranges. 2. Argon overpressure in expansion chamber.
Relatively high energy thresholds due to PSD performance	1. Improvements to light collection efficiency by adding a fourth PMT to each cell. Cell diameters are changed from 11" to 12" to fit the extra PMT.
The rubber wheels that drive the rotation of the table fail frequently.	1. Use a geared wheel with a toothed belt to prevent slippage. 2. Rather than oscillate the system which requires a lot of acceleration, rotate the entire system. To accomplish this, everything, including the computer and drive motor, must rotate as well. Power and communications will pass through a rotating coupler.
Large deadtime	1. Create multithreaded daq that integrates the readout of the encoder with data transfers from the digitizers.

7.0. REFERENCES

1. *Time-encoded imaging of energetic radiation.* **Brennan, J., Brubaker, E., Gerling, M., Marleau, P., Nowack, A., Schuster, P.** San Diego, CA : s.n., 2013. Proc. SPIE 8852, Hard X-Ray, Gamma-Ray, and Neutron Detector Physics XV. 885203.
2. *Fast Neutron Time-Encoded Imaging for Special Nuclear Material Detection.* **Nowack, A., Brennan, J., Brubaker, E., Marleau, P., Schuster, P., Steele, J.** Oakland : s.n., 2012. SORMA.
3. **Struck.** SIS3316 manual. [Online] 2013. http://www.struck.de/sis3316-2013-06-24.pdf.
4. *Maximum Likelihood Reconstruction for Emission Tomography.* **Shepp, L.A., Vardi, Y.** 2, October 1982, IEEE Transactions on Medical Imaging, Vol. 1, pp. 113-122.
5. **Padovanni, E., Pozzi, S.A., Clarke, S.D., Miller, E.C.** *Introduction to MCNPX-PoliMi Version 2.7.* 2012.

DISTRIBUTION

1	MS9406	Erik Brubaker	8127
2	MS9406	Scott Kiff	8127
3	MS9406	Peter Marleau	8127
4	MS9406	Melinda Sweany	8127
5	MS9406	Craig Tewell	8127
6	MS9292	Ken Patel	8125
7	MS9291	Jim Brennan	8125
8	MS9291	Dan Throckmorton	8125
9	MS9014	Nathalie Le Galloudec	8127
10	MS9004	Wen Hsu	8120
11	MS9004	Jim Lund	8130
12	MS1374	Kevin Seager	6831
13	MS1374	Sharon Deland	6831
14	MS0968	Robert Tachau	5753
15	MS0899	Technical Library	9536 (electronic copy)


Sandia National Laboratories